

## **Section 2**

**Data sets, diagnostic and dynamical investigations, statistical post-processing , multi-year reanalyses and associated studies**



## The passage of storms through the Eastern Mediterranean

H.A. Flocas<sup>1</sup>, I. Simmonds<sup>2</sup>, J. Kouroutzoglou<sup>1</sup>, K. Keay<sup>2</sup>, M. Hatzaki<sup>1</sup>, V. Bricolas<sup>1</sup>  
and D. Asimakopoulos<sup>1</sup>

<sup>1</sup>Department of Environmental Physics and Meteorology, Faculty of Physics,  
University of Athens, Athens, Greece

<sup>2</sup>School of Earth Sciences, The University of Melbourne, Victoria, 3010, Australia  
efloca@phys.uoa.gr

The eastern Mediterranean is a region of considerable interest with respect to many aspects cyclone behavior (e.g., intense ‘medicanes’ (Fita et al. 2009)). The region lies between the subtropics and midlatitudes, and cyclones therein obtain significant energy from both baroclinicity and surface fluxes. Additional interest arises because of the consequences of the region’s complex topography.

We have been conducting investigations of storm tracks over the Eastern Mediterranean using a sophisticated cyclone tracking scheme (Simmonds and Keay 2009) applied to the 6-hourly mean sea level pressure data in the ERA-40 reanalysis ( $2.5^\circ \times 2.5^\circ$  latitude–longitude grid) over the period 1962–2001. We analyse here some statistics for all tracks which spent at least one analysis time in the Eastern Mediterranean, here defined as the region lying within  $20^\circ$  and  $38^\circ\text{E}$ ,  $30^\circ$  and  $45^\circ\text{N}$ .

Figure 1 shows the mean annual cycle of the number storm tracks which pass through the Eastern Mediterranean. It can be seen that these tracks are most numerous from December to April; their number decreases during the warm period and tends to increase again in October. The maximum number of cyclonic tracks over the area is observed in January (11.2% of the annual total) and in March (10.3%). The minimum number of tracks occurs in July (5.3%). Figure 6 presents the interannual variation of the number of tracks within the Eastern Mediterranean region as a function of month. The total number of tracks for the 40-yr period is 10,461, translating to an average number of about 260 tracks per year. The display suggest considerable variability. In the early part of the period the number of the tracks is quite high during the cold months. The year 1969 is characterized by a peak (286) in the total annual number of tracks. Comprehensive details of this investigation can be found in Flocas et al. (2010).

### References

- Fita, L., R. Romero, A. Luque and C. Ramis, 2009: Effects of assimilating precipitation zones derived from satellite and lightning data on numerical simulations of tropical-like Mediterranean storms. *Annales Geophysicae*, **27**, 3297–3319.
- Flocas, H. A., I. Simmonds, J. Kouroutzoglou, K. Keay, M. Hatzaki, D. Asimakopoulos and V. Bricolas, 2010: On cyclonic tracks over the eastern Mediterranean *Journal of Climate*, **23**, 5243–5257.
- Simmonds, I., and K. Keay, 2009: Extraordinary September Arctic sea ice reductions and their relationships with storm behavior over 1979–2008. *Geophysical Research Letters*, **39**, L19715, doi:10.1029/2009GL039810.

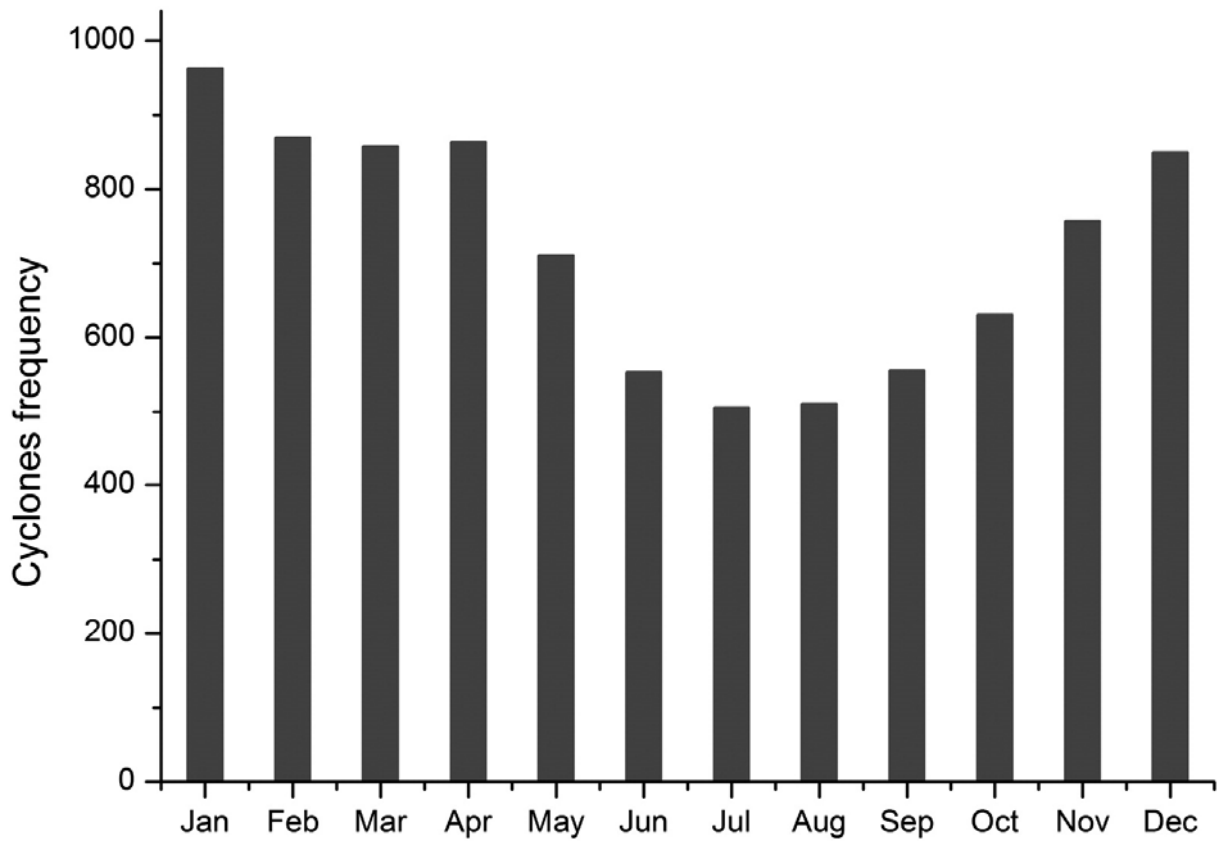


**Fig. 1:** Mean annual cycle of the number of storm tracks which pass through the Eastern Mediterranean over period 1962-2001.

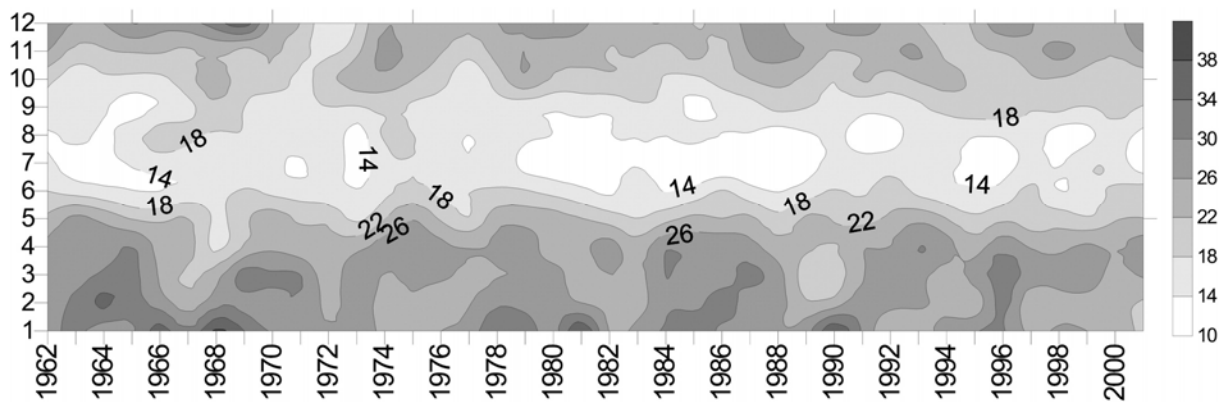


**Fig. 1:** Time series of the number of storm tracks which pass through the Eastern Mediterranean over period 1962-2001 (abscissa) as a function of month (ordinate).

## On the evolution of tropical cyclones over islands

Glebova E.S., Pokhil A.E.  
Hydrometeorological Centre of Russia  
ek.glebova@gmail.com

The influence of small pieces of land (archipelagos, islands) on tropical cyclone's configuration and structure is investigated.

The evolution of meteorological fields in tropical cyclones was calculated with mesoscale numerical model of atmosphere ETA. Two typhoons of the Pacific ocean (Ketsana and Jangmi) and two hurricanes of the Atlantic (Gustav and Hanna) were studied. Computational results for some of them are discussed below.

**Typhoon Ketsana** formed on the 25<sup>th</sup> of September (2008) nearly in the centre of the Pacific ocean and developed till the 29<sup>th</sup> of September. At first it was developing as a tropical storm, but at 0 GMT on 28.09 it reached the category of a hurricane with velocities exceeding 45 m/s. The vortex crossed Philippines and approached the Southern Chinese Sea.

Sea level pressure, wind, kinetic energy, humidity and vorticity were calculated with the ETA model.

In the pictures 1a,b the storm winds area and the kinetic energy field on the 850 hPa isobaric surface during cyclone's passage over the archipelago are shown.

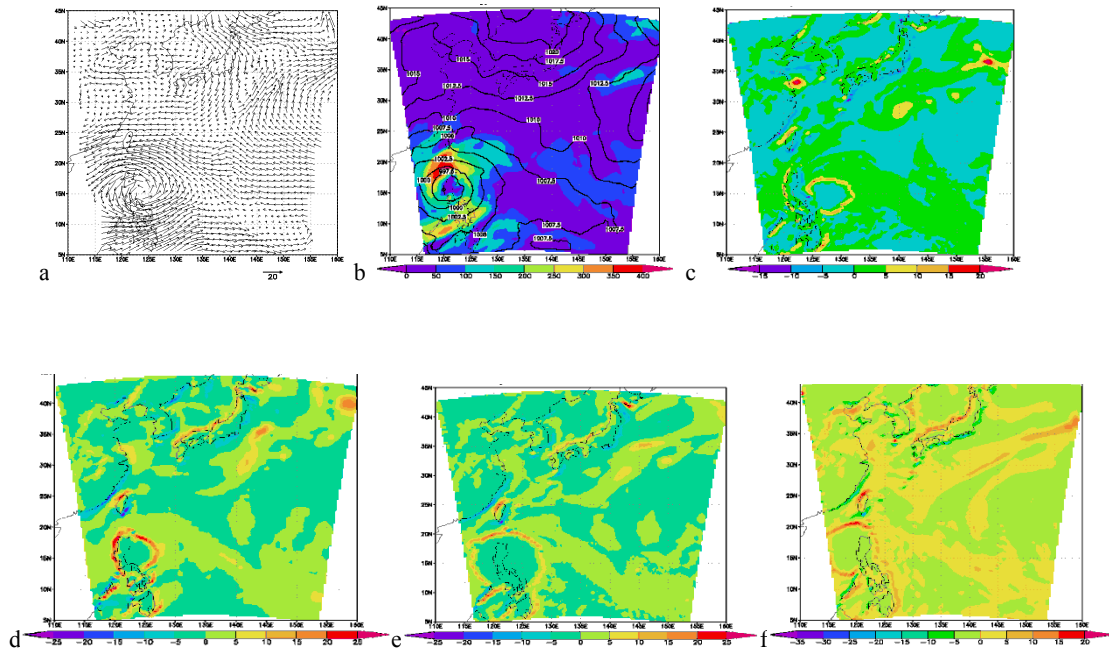
The computational results (pic.1 c,d,e,f) demonstrate clearly the vorticity field evolution. The storm winds circle and the area of the maximal vorticity have over the ocean the correct concentric form. As the typhoon approaches the land and begins moving over it, the circle loses its symmetric form, the vortex weakens strongly and, finally, the circle destroys. The energy in the part of the typhoon crossing the land is much less than the energy over the sea surface. When some parts of the cyclone have already crossed the island, the vorticity in them begins to increase (pic. 1d). Further the extension of the vorticity area is observed (pic.1e). It is accompanied by the weakness of the parts still crossing the land. The closed structure of the typhoon is destroyed due to the decrease in warm sea surface area reduction below the vortex (pic.1f).

**Typhoon Jangmi.** On the 23<sup>rd</sup> of September 2008 in the western part of the Pacific a tropical disturbance was formed. In a few hours it developed into a hurricane and was called Jangmi. On the 27<sup>th</sup> of September Jangmi became a supertyphoon with winds more than 60 m/s and with sea level pressure in the centre equal to 910 hPa. The typhoon reached Taiwan and brought heavy rains and choppy wind there. Pictures 2 a,b,c demonstrate the fields of pressure, kinetic energy and wind.

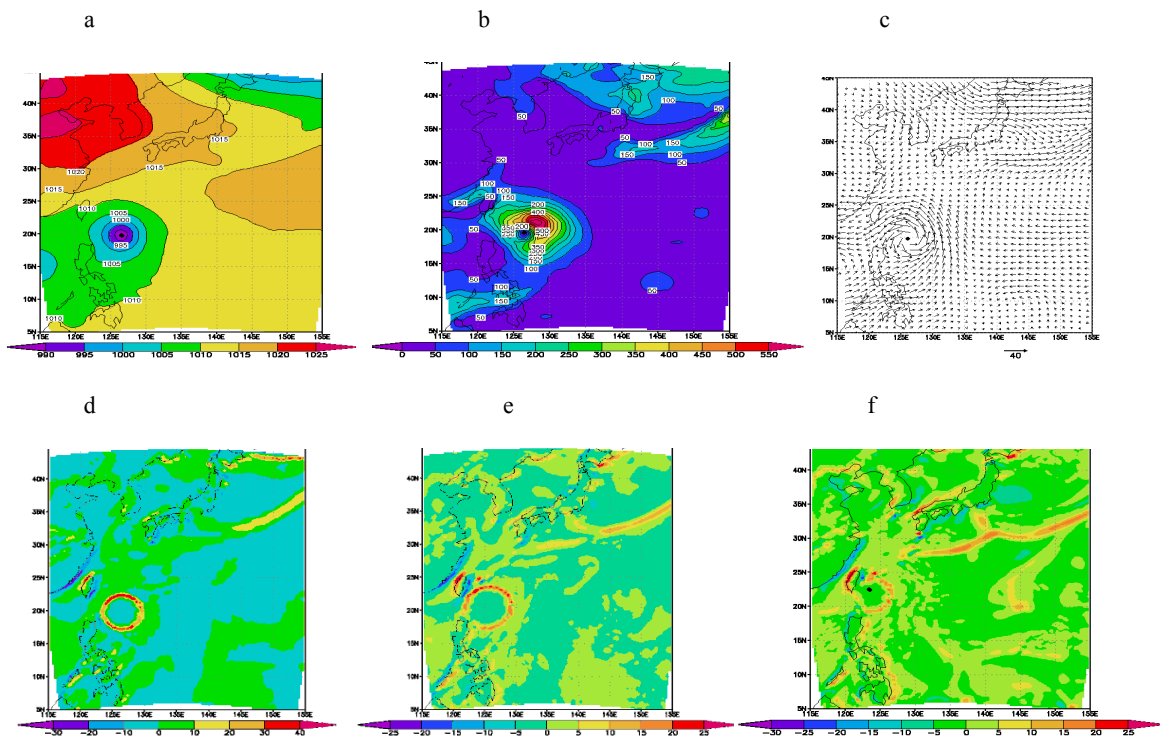
On the 25<sup>th</sup> of September the typhoon was moving over the ocean and the area of the vorticity maxima had a form of a small circle situated to the east from Philippines (pic.2d). Rapid intensification of the cyclone occurred on the 27<sup>th</sup> of September when it developed into a typhoon. At the same time a local maximum of vorticity at 1000 hPa over Taiwan appeared. (pic.2e). Typhoon's approach must have been the main reason for that. Under the influence of Philippines the storm winds circle in the south-west of the vortex was broken (pic.2e). At 12 GMT the wind circle was completely destroyed. At 18 GMT 27.09 the typhoon approached Taiwan. Strong decrease in the wind speed (to 16 m/s) and in the vorticity at 1000 hPa as well as storm wind circle's destruction was observed (pic.2f). The dynamics if the intensity was due not only to the increase in friction, but also to the relatively cold sea surface in the region. Notwithstanding this fact, the wind and the kinetic energy at 850 hPa remained high which evidences the weakness of the typhoon only near the surface.

Evolution of Caribbean hurricanes Hanna and Gustav (August 2008) over Antilles happened following the same scenario.

We can conclude that passage over even small and narrow pieces of land leads to the destruction of symmetric circulation and to considerable losses of kinetic energy in the cyclone. Kinetic energy and vorticity generation in the warm core decreases strongly due, first of all, to the decrease in horizontal pressure gradient which is caused by moving away from the warm sea surface. Returning on the ocean surface is followed by re-intensification of the cyclone.



Pic. 1. a) Real field of wind at 850 hPa at 0 GMT 26.09; b) Real field of kinetic energy at 850 hPa at 12 GMT 26.09. Calculated fields of vorticity at 1000 hPa for c) 6 GMT 25.09.; d) 0 GMT 26.09.; e) 6 GMT 26.09.; f) 18 GMT 26.09.



Pic.2. Real fields at 0 GMT 27.09: a) sea level pressure; b) kinetic energy at 850 hPa; c) wind at 850 hPa; d) corticity at 1000 hPa. Calculated fields of vorticity at e) 6 GMT 27.09 and f) 18 GMT 27.09.

# Application of scatterometer data to the diagnosis of SH mesoscale cyclones

Damien Irving<sup>1,2</sup> and Ian Simmonds<sup>1</sup>

<sup>1</sup>School of Earth Sciences, The University of Melbourne, Victoria, 3010, Australia

<sup>2</sup>CSIRO Marine and Atmospheric Research, Mordialloc, 3195, Australia

Damien.Irving@csiro.au

The analysis of mesoscale synoptic systems in mid-to-high southern latitudes is has always been a difficult task. This is in part due to their small size and relatively short lifetimes. However, these small systems are known to exert significant influence (Yuan et al. 2009).

In the investigation outlined here, we have used the surface pressure fields derived from swath of QuikSAT surface wind vectors provided by Jerome Patoux at the University of Washington (Patoux et al. 2008), the ‘UWQS pressure fields’. From these fields we have indentified and characterised (especially with respect to radius) the Southern Hemisphere mesoscale systems, using the approach detailed in Simmonds (2000) and Simmonds et al. (2008).

Over the period September 1999–November 2008 a total of 82,907 cyclonic systems were identified from the UWQS pressure fields (an average of 0.87 systems per field per swath). The radius of these systems ranged from 0.41° to 11.08° latitude (46–1230 km), where ° latitude refers to degrees of latitude, and their distribution is shown in Fig. 1. We here define mesoscale cyclones as having an upper radial bound of 4.5° latitude (500 km), the largest 15% were excluded, resulting in a set of 70,354 systems (0.74 per field). 46% of the mesoscale cyclones identified were classified as ‘open’ systems.

The mean geographical distribution of the mesocyclone frequency for each season showed an arc of highest values located 5°–10° latitude north of the sea ice (or missing data) zone, extending from the south of Africa eastward to Drake Passage (Fig. 2). Maxima within this arc were most prominent over the Amundsen and Bellingshausen Seas during summer and autumn and off the coast of Wilkes Land, south of Australia, during winter. Climatological area-weighted average system density values calculated over the entire study domain revealed autumn as the most active season, with an average of  $2.02 \times 10^{-3} (\text{° latitude})^{-2}$ . The average values for summer and winter were similar ( $1.70 \times 10^{-3} (\text{° latitude})^{-2}$  and  $1.75 \times 10^{-3} (\text{° latitude})^{-2}$  respectively), while the lowest climatological area-weighted average system density was observed during spring ( $1.40 \times 10^{-3} (\text{° latitude})^{-2}$ ). More detailed information on the structure and behavior of the identified mesoscale systems is presented in Irving et al. (2010).

Irving, D., I. Simmonds and K. Keay, 2010: Mesoscale cyclone activity over the ice-free Southern Ocean: 1999-2008. *J. Climate*, **23**, 5404–5420.

Patoux, J., R. C. Foster and R. A. Brown, 2008: An evaluation of scatterometer-derived oceanic surface pressure fields. *Journal of Applied Meteorology and Climatology*, **47**, 835-852.

Simmonds, I., 2000: Size changes over the life of sea level cyclones in the NCEP reanalysis. *Mon. Wea. Rev.*, **128**, 4118-4125.

Simmonds, I., C. Burke and K. Keay, 2008: Arctic climate change as manifest in cyclone behavior. *J. Climate*, **21**, 5777-5796.

Yuan, X., J. Patoux and C. Li, 2009: Satellite-based midlatitude cyclone statistics over the Southern Ocean: 2. Tracks and surface fluxes. *J. Geophys. Res.*, **114**, D04106, doi:10.1029/2008JD010874.

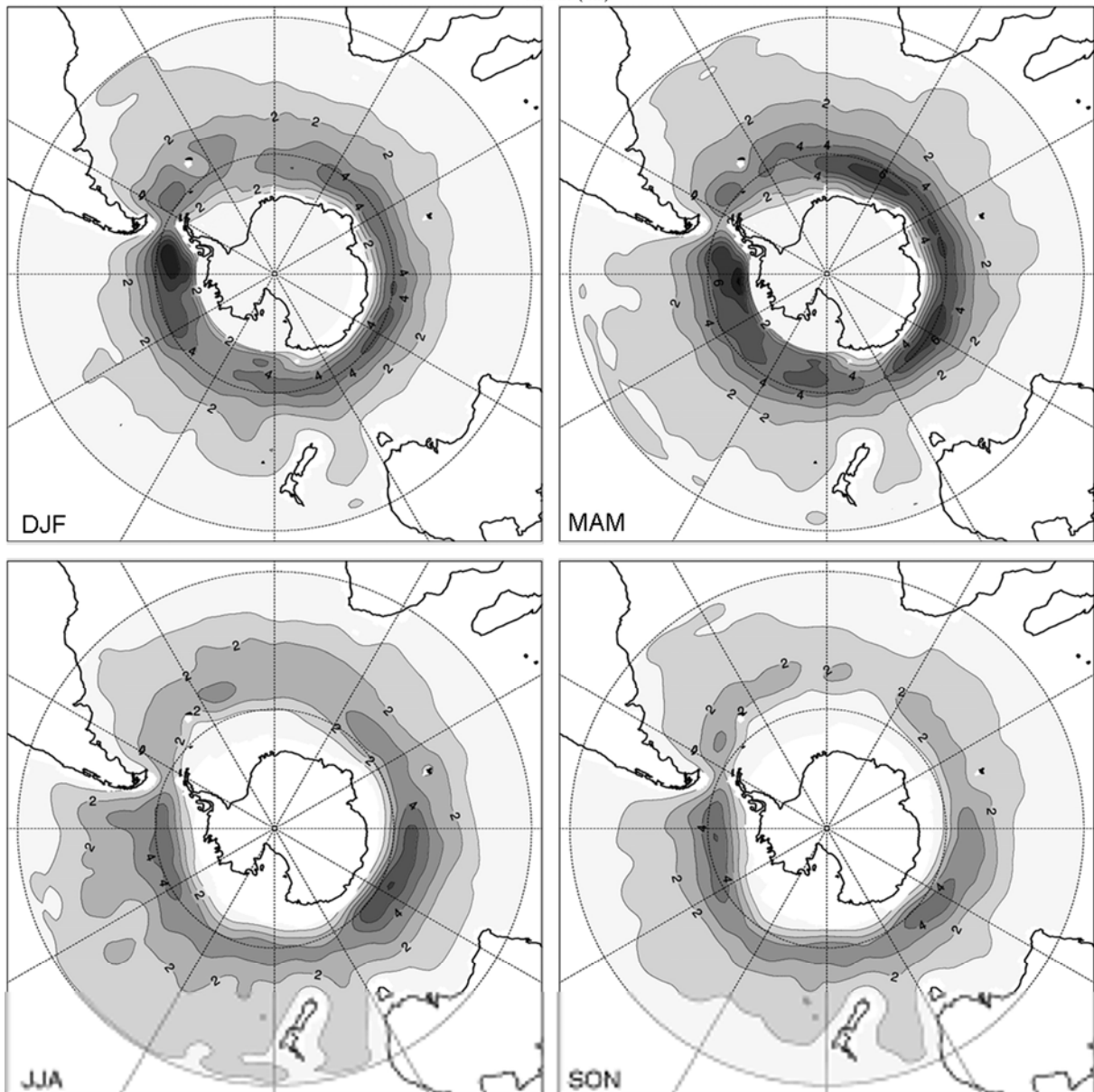
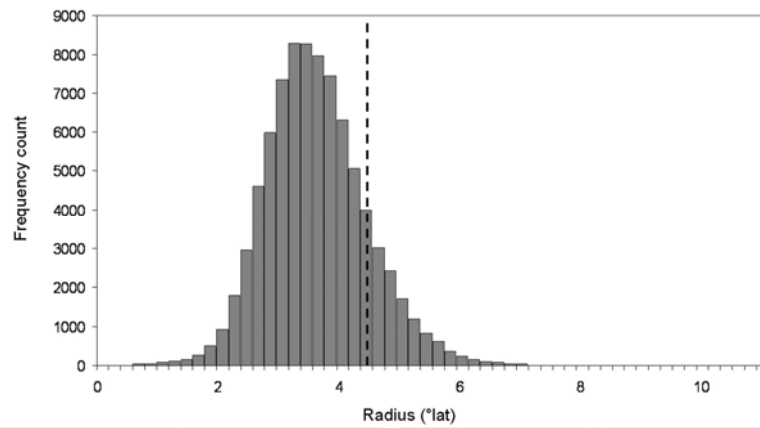


**Fig. 1 (top):** Number of systems identified per radius category. The dashed line indicates the upper radial limit ( $4.5^\circ$  latitude) for a system to be included in the climatology.

**Fig. 2 (bottom):** Mean system density (number of mesoscale cyclones found in a  $10^3 (\text{° latitude})^2$  area per analysis) for each season. The contour interval is  $1 \times 10^{-3} (\text{° latitude})^{-2}$ .

# Reproducibility of diurnal variation of summertime precipitation by a nonhydrostatic model

Masaomi Nakamura\*, Teruyuki Kato and Syugo Hayashi

\*Meteorological Research Institute, Tsukuba, Ibaraki, 305-0052, JAPAN

manakamu@mri-jma.go.jp

## 1. Introduction

The Kanto District, located in central Japan, consists of the Kanto Plain and mountainous areas in the north and west and it faces the Pacific Ocean in the south and east. Due to its geographical features, convective precipitation associated with thermally-induced circulation are frequently observed in the afternoon and evening in summer. Many authors investigated the characteristic of these convective activities from observational point of view. On the other hand, studies from reproducibility or forecasting aspects by using numerical models are very limited.

Summertime convective precipitation is one of important targets of forecast in the Kanto District and to evaluate the performance of numerical model and to clarify the problem in reproducing it, if exists, is an interesting work still left. In this study, we evaluate the reproducibility of observational characteristics in the diurnal variation of summertime precipitation around the Kanto District, based on one-month simulation results by the Japan Meteorological Agency (JMA) NonHydrostatic Model (hereafter referred to as NHM).

## 2. Experimental design

First, NHM was run at 5-km grid spacing from 03 to 21 JST (Japan Standard Time), with initial and boundary conditions given from JMA operational mesoscale analysis of 3-hourly intervals. Then, NHM was run at 1-km grid spacing from 04 to 21JST with initial and boundary conditions given from the NHM5km results. The experiments were carried out for one month of August 2010.

The specifications of NHM5km and 1km are nearly the same. Both models use Mellor-Yamada level-3 scheme improved by Nakanishi and Niino and cloud microphysics predicting both the mixing ratio and number density of water cloud, ice cloud, rain, snow and graupel. Both models have horizontal grid numbers of 500 and 400 in the x and y directions, respectively, and stretched 50 vertical layers with a depth of 40m near the surface and about 900m at the model top (~22km). A big difference between the two models is in that NHM5km uses the Kain-Fritsch cumulus convection scheme, while NHM1km does not. Details of NHM are described in Saito et al. (2007) and literatures cited there.

## 3. Results

Figure 1 shows the horizontal distribution of the frequency of precipitation (hereinafter abbreviated as FP) from observation and NHM1km. The observation data, JMA radar-raingauge analyzed precipitation (referred to as AP) which originally has an horizontal resolution of 1km, and NHM1km results are used after being spatially averaged over 5km-square grid. FP is obtained by counting the number of hourly precipitation exceeding 1mm at each 5km-grid point during a 3-hour period, 15-16, 16-17 and 17-18JST for each day and then averaging over the month. The figure indicates that the model fails to reproduce an increase of FP over the northern mountain area in the late afternoon.

FP of NHM1km increases from 12JST to 15JST, following that of observation (AP), but stops increasing

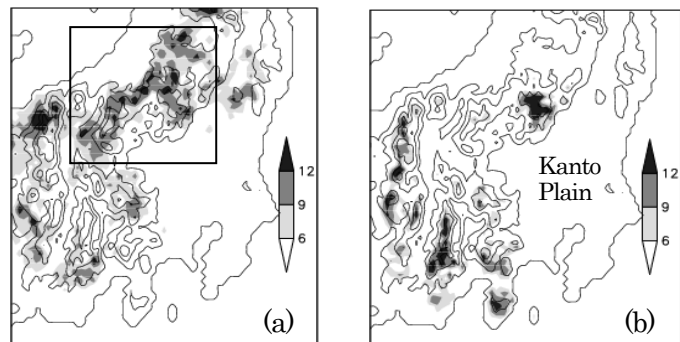


Figure 1. Observed (a) and NHM1km's (b) monthly mean frequency of hourly-precipitation exceeding 1mm on the 5-km grid. Contours are drawn at 500m intervals. The whole domain, including the Kanto District, is that of NHM1km.

afterwards (Fig.2a). The diurnal increase of precipitable water (dPW) of the model is not enough (fig.2b); dPW is defined as an increment of PW from a value at 06JST, nearly when PW has a minimum value. The negative bias of dPW increases toward peak time of around 18JST. The scatter diagram for the region including the northern mountain area (Fig.3) indicates that, irrespective of geographical location, plain or mountain, model's PW has a negative bias.

Figure 4 shows that the horizontal distribution of the bias of model-predicted PW at 18JST; model's PW is corrected for the difference between model topography and GPS station heights by a rate 1.5mm/100m (roughly estimated from Fig.3). Positive-bias points are seen only over southern coastal areas. The model has a negative bias in other area. Considering the fact that a diurnal increase of PW is mainly caused by transport of water vapor from low altitude areas to mountains and to upper layers there, Figures 2b and 3 suggest that there is a possibility that the model does not have sufficient ability to transport water vapor to higher-altitude layers.

If we draw figures similar to Fig.3 and 4 for initial hours, it is seen that model's PW is insufficient even for these hours, though less in amount compared to later hours. The insufficient initial PW could affect the following time evolution of the model.

#### 4. Summary and concluding remarks

- 1) NHM fails to reproduce summertime precipitation peak in the late afternoon, especially over the northern mountain area in the Kanto District.
- 2) The model also underestimates PW over the area, compared with GPS observation. PW of the model is an underestimate, even in initial hours.
- 3) This bias in the initial field could affect the time evolution of model fields and cause insufficient peaks in FP and PW in the model, but an possibility that they are caused by some defects in the model could not be denied.
- 4) The result of NMM5km is not described here, but it shows essentially the same features as NHM1km.

It is left for future study to identify factors causing NHM's FP and PW errors and improve its reproducibility for summer-time convective precipitation.

#### 5. References

Saito, K., J. Ishida, K. Aranami, T. Hara, T. Segawa, M. Narita, and Y. Honda, 2007: Nonhydrostatic atmospheric models and operational development at JMA. *J. Meteor. Soc. Japan*, **85**, 271-304.

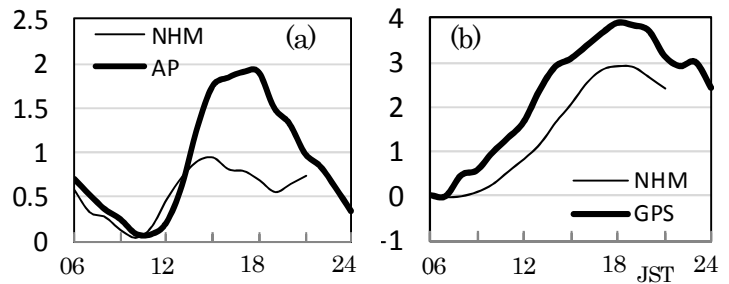


Figure 2. (a) Diurnal variation of monthly-mean frequency of hourly-precipitation exceeding 1mm, averaged over the 5km land grids within the rectangular region in Fig.1a. Thick and thin solid lines represent observation and NHM1km results, respectively. (b) Same as (a) but for monthly mean dPW (mm) averaged over GPS points.

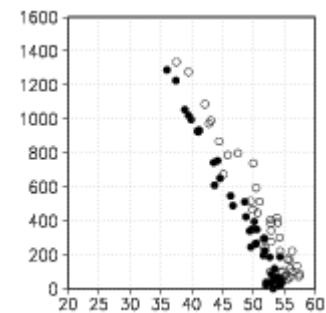


Figure 3. Scatter diagram for monthly mean PW (mm) and station height (m) for GPS (open circle) within the rectangular region in Fig.1a and for NHM1km (filled circle) at 18JST.

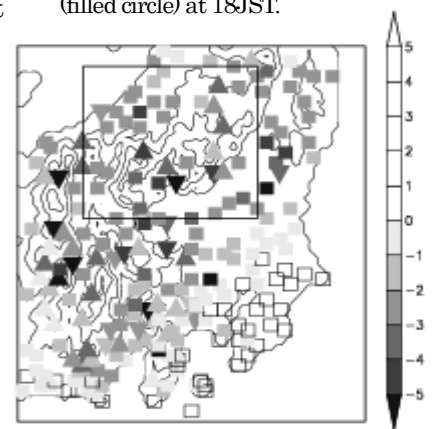


Figure 4. Monthly mean NHM1km-minus-GPS PW at 18JST.  $\Delta$ ( $\nabla$ ) represents a point where the model topography is higher (lower) than GPS-station height by more than 100m.  $\square$  otherwise. Positive values are white colored.

# Investigation and movement of tropical cyclones interacting with each other and with different atmospheric structures based on the ETA-model calculations

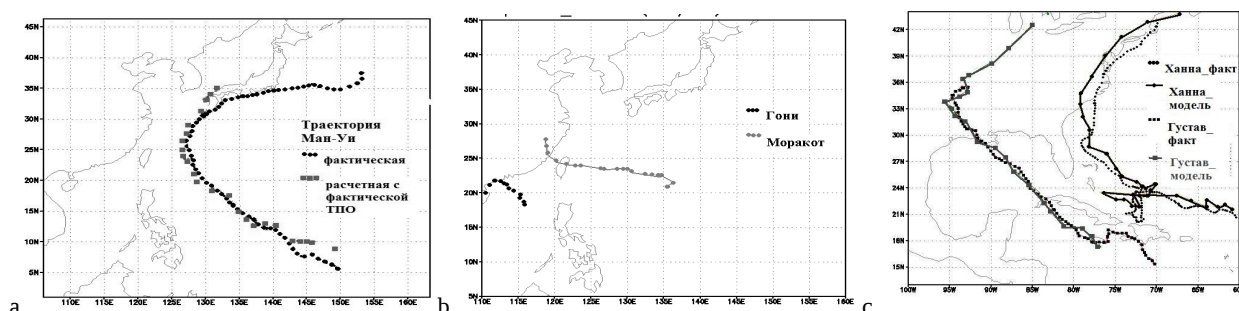
Pokhil A.E., Glebova E.S.

Hydrometeorological Centre of Russia  
ek.glebova@gmail.com

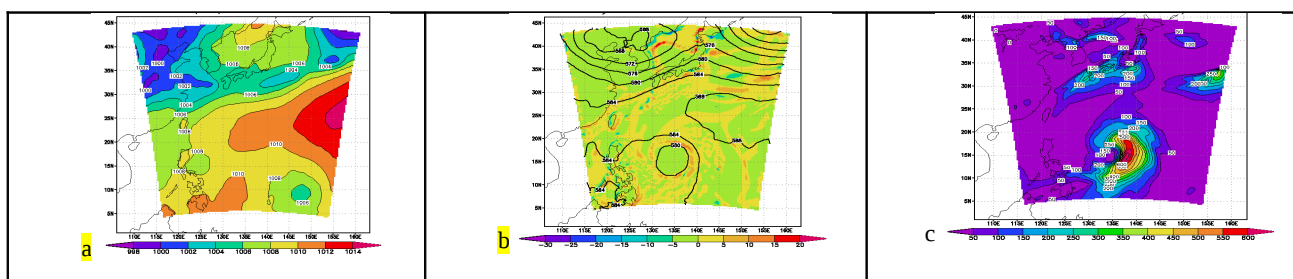
The dynamics of typhoons Man-Yi and Morakot interaction with polar fronts is discussed in the current paper, as well as the meteorological fields evolution in hurricanes Hanna and Gustav which developed simultaneously. Simulation of meteorological fields evolution in tropical cyclones was produced by mesoscale numerical ETA model of atmosphere. The model was integrated with a horizontal step equal to 22 km and a time step equal to 90 seconds. NCEP analysis data with 1° resolution was used to create initial and boundary conditions. The fields of 5-day average sea surface temperature were taken to define sea surface temperature (SST). Real and simulated trajectories of investigated tropical cyclones are shown in the picture 1a.

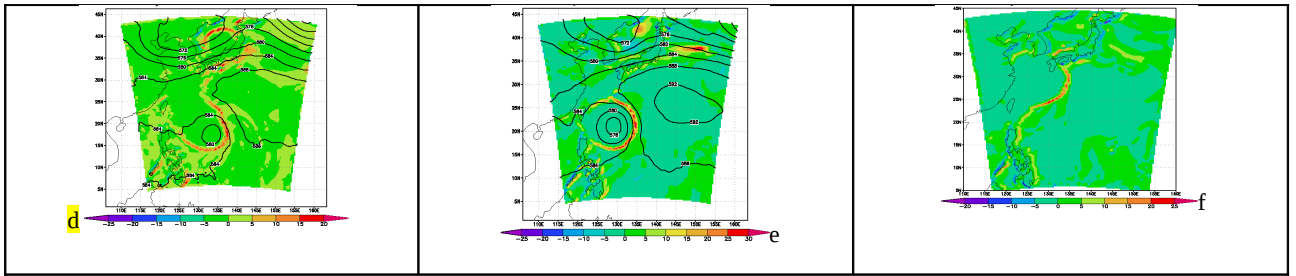
The analysis of calculation results demonstrated that:

1. The model is good at simulation of meteorological fields dynamics during TC's evolution,
2. It can be clearly seen that the structure and configuration of vortices change significantly in the course of their interaction with each other, with the polar front or during their passage over the islands (pic.2,3,4).
3. The process of TC (Man-Yi) and polar front interaction is accompanied by deformation of the vortical zone; by break of the vorticity ring and its mergence with polar front's vortical area, by appearance of a so-called 'convective tail', taking part in the interaction with a frontal zone (pic.2). Besides that, a considerable increase in the velocity of storm's centre is observed.
4. The moment of beginning of interaction between tropical cyclones and a polar front and, correspondingly, the moment of possible turn of trajectory can be defined from fields of sea-level pressure and vorticity. The same is fair for cases of tropical cyclones' interaction with each other (in our case it's Morakot and Goni) (pic.3).
5. The dynamics of kinetic energy fields at 850 hPa demonstrates the process of energy transfer from one structure to the other (Gustav - Hanna): intensification of one cyclone and energy losses in the other (pic.4).
6. The islands (Greater Antilles) influence on a hurricane (Gustav) leads to transformation of TC's fields structure in TC: break of circulation system and of symmetry of vorticity, velocity and kinetic energy fields (pic.4).
7. The considerable influence of SST on TC's characteristics is proved.
8. It is shown that the atmosphere in some point reacts on formation and movement of a vortex situated in 2000 km from this place.

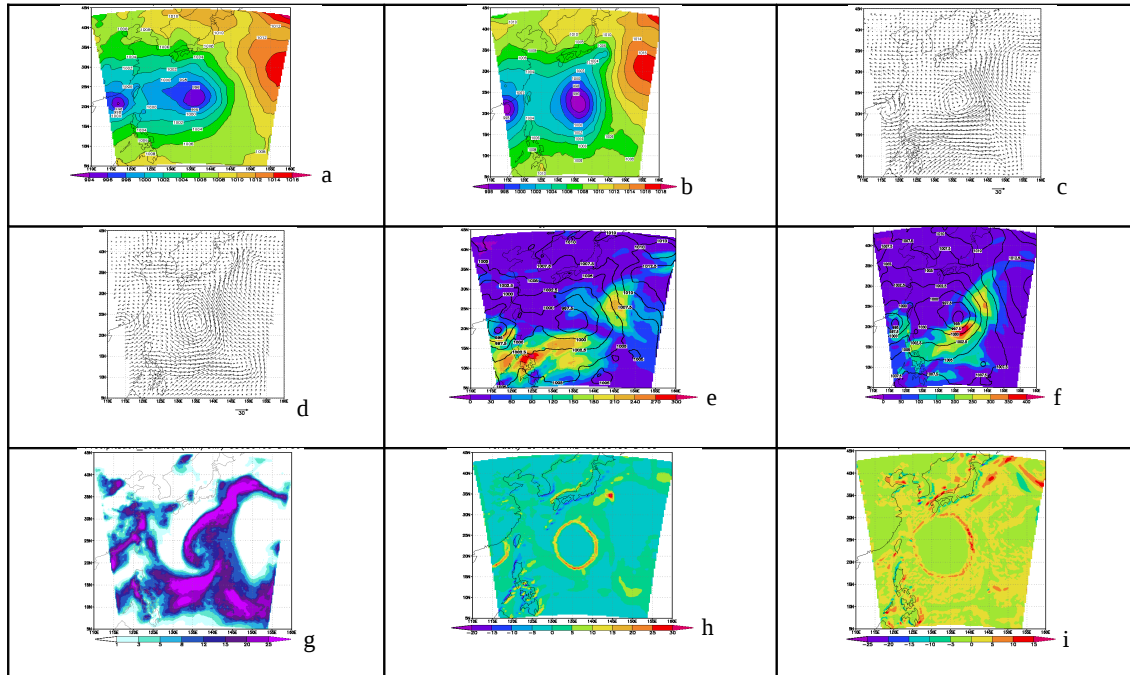


Pic.1. a) Real and simulated trajectory of tropical cyclone Man-Yi, b) Real and simulated trajectories of tropical cyclones Goni and Morakot, c) Real and simulated trajectories of tropical cyclones Gustav and Hanna.

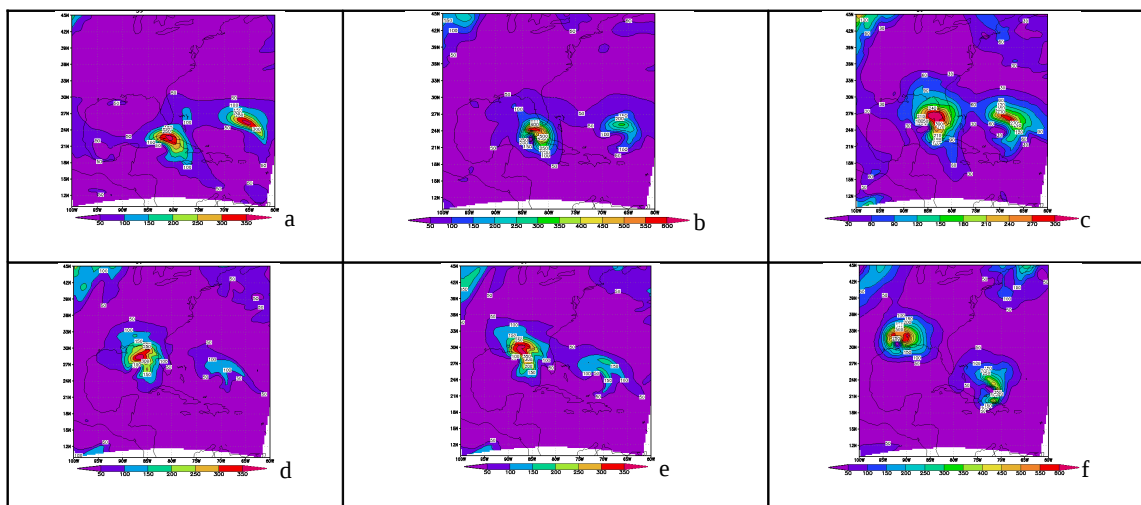




Pic. 2. Calculated meteorological fields in tropical cyclone Man-Yi a) sea-level pressure 8.07.2007; b,d,e,f) vorticity at 1000 hPa 10,11,12, 13.07.2007 correspondingly b) kinetic energy 10.07.2007.



Pic.3. Calculated meteorological fields in TC Goni and Morakot: a,b) sea-level pressure at 18 GMT 3.08.2009 and at 0 GMT 4.08.2009 correspondingly; c,d) velocity at 850hPa at 18 GMT 3.08.2009 and at 12 GMT 4.08.2009 correspondingly; e,f) kinetic energy at 850 hPa at 6 and 18 GMT 3.08.2009 correspondingly; g) precipitation at 6 GMT 4.08.2009; h,i) vorticity at 1000 hPa at 0 and 18 GMT 4.08.2009 correspondingly.



Pic. 4. Calculated fields of kinetic energy at 850 hPa during interaction of tropical cyclones «Hanna» and «Gustav» a,b,c) 30.08.2008 at 12 GMT, 31.08.2008 at 0 and 12 GMT correspondingly; d,e,f) 31.08.2008 at 24 and 30 GMT and 2.09.2008 at 0 GMT correspondingly.

## Dramatic effect of small scale SST South Atlantic features on the evolution of Hurricane Catarina

M. L. Vianna<sup>1</sup>, V. V. Menezes<sup>2</sup>, A. B. Pezza<sup>3</sup>, and I. Simmonds<sup>3</sup>

<sup>1</sup>VM Oceânica LTDA, San Jose dos Campos, Brazil

<sup>2</sup>VM Oceânica LTDA, Arraial do Cabo, Brazil

<sup>3</sup>School of Earth Sciences, The University of Melbourne, Victoria, 3010, Australia  
marcio@vmoceanica.com.br

The development and evolution of the first recorded South Atlantic hurricane (Catarina) in March 2004 is still attracting much interest (Pezza and Simmonds 2005, 2008, McTaggart-Cowan et al. 2006, Veiga et al. 2008, Pezza et al. 2009, Pereira Filho et al. 2010). One puzzle was as to why it evolved over waters with homogeneous (Reynolds) sea surface temperatures (SST) of 24°C.

Figure 1a shows the SST distribution in the region immediately before Catarina was formed on 19 March, overlaid with the future track of Catarina. Along the track all SSTs were below 26°C south of 26°S, and there is no strong evidence of mesoscale ocean features in the vicinity of that track.

By contrast, the distribution of sea surface height (SSH) (retrieved from satellite altimeters) reveals clear eddy structures present under the future Catarina track (Figure 1b). The most notable are three ‘warm core rings’ (WCRs) in a ridge-like distribution located around 27–31°S and 40–45°W (WCR-1, WCR-3 and WCR-4), and an eastern WCR centered at 30°S–36°W (WCR-2). These 200–300 km features were present almost without change since the end of February 2004. Figure 2c shows the map of altimeter-derived 17°C isotherm depth (D17) on 19 March. WCR-1 to 4 have D17s at least 70 m greater than the background value of 100 m. (D17 is much shallower near the shelf slope, where it may be less than 30 m.) The final panel in Figure 1 shows the derived absolute geostrophic current field for 19 March. The mesoscale circulations show currents and eddies with speeds of 30 cm s<sup>-1</sup> in the open ocean, and southward flows of up to 40 cm s<sup>-1</sup> well inside the continental shelf.

Our analysis supports suggestions that high resolution SST of central importance in accounting for hurricane formations and development. We present in Vianna et al. (2010) a comprehensive analysis of the extraordinary Catarina system.

### References

- McTaggart-Cowan, R., L. F. Bosart, C. A. Davis, E. H. Atallah, J. R. Gyakum and K. A. Emanuel, 2006: Analysis of Hurricane Catarina (2004). *Mon. Wea. Rev.*, **134**, 3029-3053.
- Pereira Filho, A. J., A. B. Pezza, I. Simmonds, R. S. Lima and M. Vianna, 2010: New perspectives on the synoptic and mesoscale structure of Hurricane Catarina. *Atmospheric Research*, **95**, 157–171.
- Pezza, A. B., and I. Simmonds, 2005: The first South Atlantic hurricane: Unprecedented blocking, low shear and climate change. *Geophys. Res. Lett.*, **32**, L15712, doi: 10.1029/2005GL023390.
- Pezza, A. B., and I. Simmonds, 2008: Large-scale factors in tropical and extratropical cyclone transition and extreme weather events. *Annals of the New York Academy of Sciences*, **1146**, 189-211.

- Pezza, A. B., I. Simmonds and A. J. Pereira Filho, 2009: Climate perspective on the large-scale circulation associated with the transition of the first South Atlantic hurricane. *Int. J. Climatol.*, **29**, 1116-1130.
- Veiga, J. A. P., A. B. Pezza, I. Simmonds and P. L. Silva Dias, 2008: An analysis of the environmental energetics associated with the transition of the first South Atlantic hurricane. *Geophys. Res. Lett.*, **35**, L15806, doi:10.1029/2008GL034511.
- Vianna, M. L., V. V. Menezes, A. B. Pezza and I. Simmonds, 2010: Interactions between Hurricane Catarina (2004) and warm core rings in the South Atlantic Ocean. *J. Geophys. Res.*, **115**, C07002, doi:10.1029/2009JC005974.

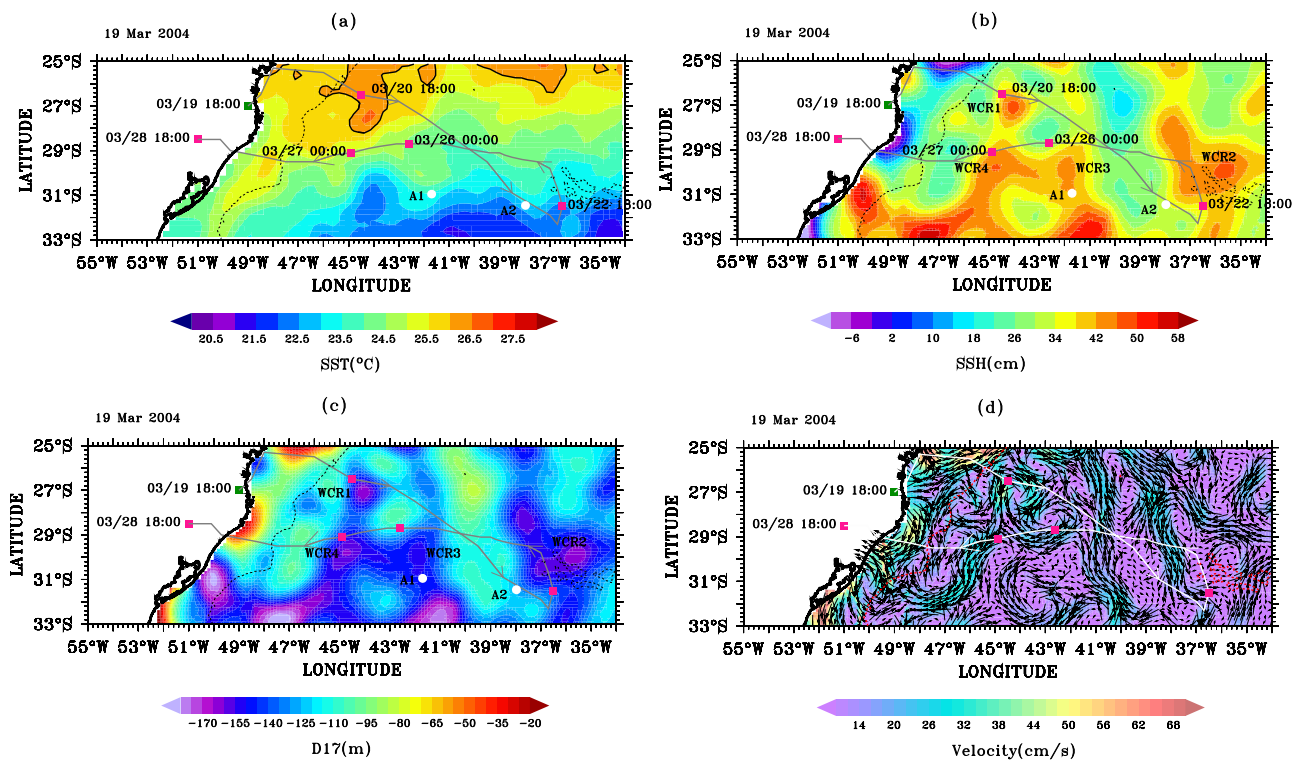


**Figure 1:** SST, SSH, D17, and geostrophic currents on 19 March, 1 day before the onset of the Catarina storm, overlaid with the future centroid track of Catarina: (a) Reynolds SST exhibiting only one tongue with 26°C over a background of lower temperatures south of 27°S. (b) The SSH data showing the complex ocean topography featuring four main WCR signatures traversed by the track, with two nearby Argo floats at positions A1 (over WCR-3) and A2 away from any WCR. (c) D17 subsurface isotherm. (d) The mesoscale absolute geostrophic currents (small vectors refer to less than 10 cm s<sup>-1</sup>). Red squares denote daily storm center positions, and dotted line is the 1000 m depth isobath.